Two-dimensional Nanoarchitectonics for Two-Dimensional Materials: Interfacial Engineering of Transition Metal Dichalcogenides

Pragati A. Shinde[a] *and Katsuhiko Ariga*[a,b]

[a]Research Center for Materials Nanoarchitectonics, National Institute for Materials Science (NIMS), 1-1 Namiki, Tsukuba 305-0044, JAPAN

[b]Graduate School of Frontier Sciences, The University of Tokyo, 5-1-5 Kashiwanoha, Kashiwa, Chiba 277-8561, JAPAN

Abstract: Transition metal dichalcogenides (TMDs) have been attracted increasingly attention in fundamental studies and technological applications owing to their atomically thin thickness,

expanded interlayer distance, motif bandgap, and phase transition ability. Even though TMDs own a wide variety of material assets from semiconductor to semimetallic to metallic, the materials with fixed features may not show excellence for precise application. As a result of exclusive crystalline polymorphs, physical and chemical assets of TMDs can be efficiently modified via various approaches of interface nanoarchitectonics, including heteroatom doping, heterostructure, phase engineering, reducing size, alloying, and hybridization. With the modifying properties, TMDs become interesting materials in diverse fields, including catalysis, energy, electronics, transistors, and optoelectronics.

1 Introduction

Since the successful preparation of graphene, two-dimensional (2D) materials having exclusive physical and chemical assets attracted much interest for potential applications in catalysis, energy, electronics, transistors and optoelectronics[1-4]. From the library of 2D materials, TMDs have recently attracted the attention of scientific research and industries owing to their exclusive crystal structures and different material properties[5-7]. TMDs are generally denoted as MX_2, where M represents transition metal squeezed in two chalcogen X (X: S, Se, and Te) atoms in a single cell[8]. Metals from groups 4 to 10 have different numbers of electrons in their d orbital and filling,

resulting in diverse electronic assets such as insulator, semiconducting, semimetallic, metallic and superconductors[9-11]. The comprehensive series of electronic properties not only lift the progress of TMDs in electronics and optoelectronics but also enable promising bids in catalysis and energy [12-15]. Furthermore, different TMDs atomic arrangements are vital in defining material properties[16]. In monolayer TMDs, the metal-chalcogen bond is covalent, whereas after several TMD layers stacked, it forms bulk TMD material[17]. Here, weak van der Waals forces hold the neighboring layers together[7, 18]. The weak interactions between layers are overwhelmed via the exfoliation process to get thin sheets[19-20]. Additionally, variations in chemical bonding and crystal structure of metal atoms lead to diverse crystalline phases of TMDs.

Furthermore, the fiery popularity of TMDs relies not only on their inherent properties but also on tunable electrical and electrocatalytic performance[21-22]. Because of the high anisotropy and exclusive structural polymorphs, features of TMDs are efficiently modified through different strategies of interface engineering, including heteroatom doping, heterostructure, phase engineering, reducing size, alloying, and hybridization[17, 23-24]. For example, through phase engineering, 2H semiconducting TMDs can be converted into 1T metallic TMDs, leading to high electronic conductivity[25]. The alternative instance is via the incorporation of heteroatoms or

doping, charge carrier in TMDs can be modified. Recent technologies as well as devices need an inclusive collection of fine material properties, which can barely be found in a solitary material deprived of tuning. Thus, the 2D TMDs offer a giant platform for modifying the material properties to anticipate functionality, further appealing to excessive courtesy and inaugural prospects for diverse applications. This review summarizes current advancements in interface nanoarchitectonics of TMDs, mostly converging assets at the interface.

2 Crystal Structures of Transition Metal Dichalcogenides (TMDs)

In a post-graphene decade, TMDs are the furthermost prevalent family of 2D layered materials because of their fascinating electronic assets and broad utilization in various arenas. For TMDs, one unit cell is three atoms thick where transition metal in each monolayer squeezed in two chalcogens, forming stoichiometric (MX_2)[26]. The interlayer bonds in TMDs are covalent, whereas the interlayer bonds between two MX_2 are generally van der Waals[27]. TMDs have diverse atomic arrangements, and their novel electrical properties in different polymorphs are mostly interrelated to their performance[28]. TMDs exist in different phases depending on the coordination of M and X atoms ((Figure 1a-e)[23] , including the thermodynamically stable 2H phase with trigonal prismatic synchronization of metal atoms in each layer, where the multiple layers are stacked in the AB order

[29]. The analogous atomic arrangements like 2H phase form 3R TMDs, but the location of M and X atoms shifted, leading to a diverse stacking order of ABC in unit cell[18, 30]. In disparity, 1T phase TMDs own octahedral coordination of M atoms with AA stacking order [19]. The 1T TMDs can be simply changed to distorted octahedral 1T'. Because of the difference in electronic structure, 2H polymorph is semiconducting with bandgap of 1.2 – 1.9 eV, while the 1T/T' polymorph is metallic[31]. As the number of electrons in outer orbitals changes, total electron energy also changes, resulting in phase transition from 2H to 1T and 1T', respectively[32]. Thus, the electron number in d orbital and atomic arrangement of metal determines the phase, which significantly determines the assets of TMDs[8].

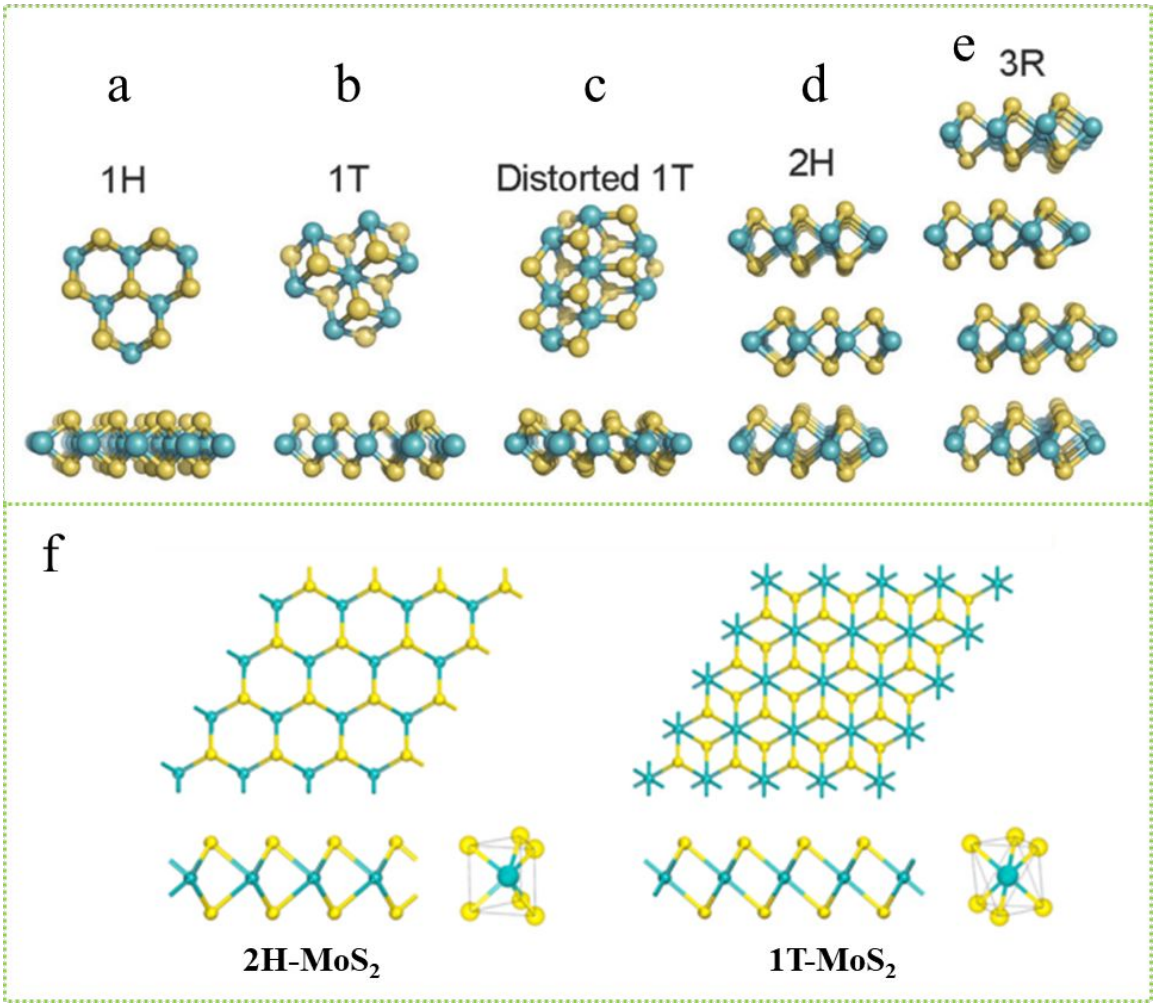

Figure 1. Atomic structures of different polymorphs of TMDs a) 1H-MX_2, b) 1T-MX_2, c) distorted 1T-MX_2, d) 2H-MX_2 and 3R-MX_2. Reprinted with permission from. Ref.[23]. Copyright 2015 Royal Society of Chemistry. d) top and side sights of 2H MoS_2 and 1T MoS_2 monolayer. Reprinted rom ref.[33]. Copyright 2015 American Chemical Society.

The 2H polymorphs in TMDs is semiconducting and stable, whereas the 1T/T' polymorphs is metastable with high electrical conductivity[34]. Nevertheless, 1T/T' polymorphs undergo a phase

conversion from 1T/T' to 2H phase due to the surface atoms reordering, and reverse progression is recognized as exciting with a high alteration barrier; hence, TMDs are naturally found in 2H phase[35]. Experimental and theoretical studies confirm that the in 2H TMDs edge sites are electrochemically active for electrochemical reactions, whereas basal planes are chemically inactive[21, 36]. In contrast, basal planes are more functional for 1T/T' TMDs, as edge and in-plan atoms are energetic in 1T/T' polymorphs rather than only edges in 2H TMDs[37]. In MoS_2, the individual unit cell comprises Mo atoms squeezed in two S atoms. Based on atomic arrangement (S-Mo-S), MoS_2 is commonly observed in two crystalline phases, 1T and 2H. As seen in Figure 1d, a single Mo was bounded by six S atoms in both polymorphs. In 2H MoS_2, Mo atoms are prismatically synchronized to S atoms in top and bottom planes, whereas in 1T phase MoS_2, Mo atoms coordinated octahedrally with S layers and S atoms in top and bottom planes are balanced[33].

3 Engineering Strategies of Interfaces

In recent years, TMDs have offered a huge platform for scientific research and their practical applications in electronics, catalysis, and energy storage fields[38]. Various efficient methods have been developed to fully exploit their potential to produce TMDs with desired phase structure, mixed phase, and defects. Distinct from bulk materials, 2D TMDs are interface-type materials, and

their performance for particular applications is structured and revealed by the interface. The TMDs crystal deepened with inherent defects like vacancies, grain boundaries, and substitutional impurities. The presence of such defects indicates a noteworthy influence on the electrical conductivity and performance activity of TMDs based devices. Therefore, is necessary to develop different strategies of defect and interface engineering to accomplish materials with unique features and high performance. The interface nanoarchitectonics enables carrier transport, persuades successful doping, and amends the band structure and phase modulation in TMDs; based on which multifunctional heterostructures can be constructed. With this, understanding the role of the interface and developing efficient interface engineering strategies is of great influence for further developments of TMDs-based electronics, optoelectronics, transistors, catalyst and energy storage devices. The investigation of actual approaches to tune basal planes of TMDs is significantly vital for the imminent progress of such an auspicious library of compounds. Figure 2 shows a schematic illustration for different strategies of interface nanoarchitectonics in TMDs.

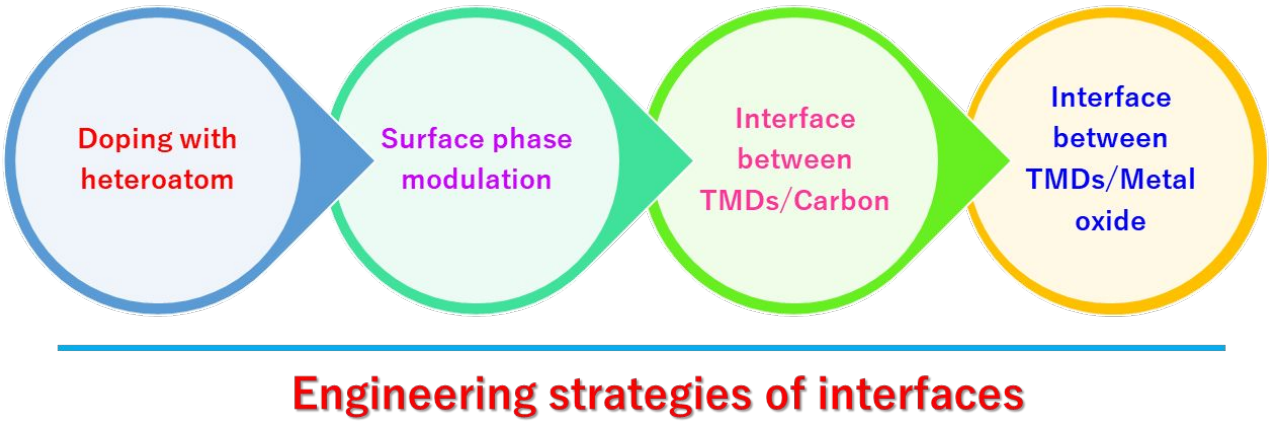

Figure 2. Schematic design for the different approaches of interface nanoarchitectonics in TMDs.

3.1 Doping with Heteroatoms

Doping is an active technique to skill the properties of TMDs via incorporating impurities. TMDs have different properties extending from insulating to semiconducting to metallic. Doping in TMDs is a capable method to alter the structure and electrical, optical, magnetic, and electrochemical properties of TMDs via altering band alignment[39]. In TMDs, dopant atoms are introduced in layers or change the structure to form a different phase. Substitution of dopant atoms can be a direct substitution in lattice or interstitial regions in existing atoms in a lattice of TMDs[40]. For catalysis and energy applications, doping increases electroactive sites by altering the surface architecture to interpret formation of additional active sites e.g., basal plane of TMDs, thus enhancing the catalytic and energy storage performance[41-42]. MoS_2 is a promising material for

catalysis and storage applications; however, boundaries associated with its low electrical conductivity and few surface-active sites restrict its performance[43]. Among the numerous approaches employed to improve the activity of MoS_2, one effective strategy is heteroatom metal doping in MoS_2 lattice to improve the number of active sites. Until now, different metal intercalated MoS_2 has been stated, including Co-doped MoS_2[44], Ni-doped MoS_2[45], Pd-doped MoS_2[46] and P-doped MoS_2[47]. Li and coworkers doped Pt in MoS_2 and achieved fractional phase transition of MoS_2 from 2H to 1T phase, leading to enhanced HER performance[48]. The metal doping into MoS_2 gives phase transition, enhances electrical conductivity, and decreases charge-transfer resistance[49-51]. The flower-like MoS_2 was seen in the TEM image (Figure 3a). The STEM showed two crystallographic phases in Pt-doped MoS_2, 2H and 1T MoS_2 (Figure 3b). The downshifts in S 2p and Mo 3d spectra demonstrated successful 2H to 1T phase transition (Figure 3c, d). Such a phase transition after doping might be caused by an electron donated from the Pt atom after doping into MoS_2 lattice. DFT optimized structures showed three possible Pt doping sites in MoS_2 (Figure 3e-g). DFT analysis again revealed that S species next to Pt in MoS_2 acted as furthermost active regions for HER (Figure 3h-j). Even though most of the reports showed that doping into TMDs increases the performance of materials with great improvement in conductivity

of TMDs, however heavily doped electronegative dopants such as phosphorus cause low conductivity owing to the delocalized electrons in metal[52]. Song et al.[52] in their recent work, demonstrated that during phosphorus doping, reaction time, temperature and percentage of phosphorus was essential to achieve more benefits as P doping into MoS_2 at low temperature retain the morphology. On the other hand, Yacaman et al.[53] utilized red phosphorus for P doping into MoS_2 lattice at 900 °C, that caused ruin of MoS_2 morphology. Furthermore, Li et al.[54] reported fabrication of 1T@2H MoS_2 homojunction and achieved high activity for supercapacitors. Te thermal treatment of MoS_2 led to formation of 1T@2H MoS_2 (Figure 3k). Authors verified that Te intercalation in MoS_2 lattice triggered the interlayer expansion, offered high conductivity, and facilitated charge transportation and ion diffusion. 1T@2H MoS_2 showed 6-10 layers with increased interlayer distance of 0.64 nm than the bare 2H MoS_2 (0.615 nm) with two distinct lattice regions corresponding to 1T MoS_2 and 2H MoS_2, respectively (Figure 3l). Some crystalline phase deformation and defects were observed after Te doping, which helps to enhance electrochemical performance (Figure 3m). Liu and coworkers[55] designed P intercalation into MoS_2 nanosheets to incorporate electroactive sites on the basal plane, increase interlayer spacing, and utilized P-doped MoS_2 for electrocatalysis. The excellent HER activity was achieved with a Tafel slope of 34

mV/dec and a small overpotential of 43 mV. Similarly, Shi et al.[56] developed Co-doped tungsten oxide first and then converted oxide into sulfide by sulfurization. The obtained Co-doped WS_2 showed excellent HER activity with an overpotential of 210 mV at 10 mA cm^{-2}.

The thermal stability of TMDs is lower than that of conventional semiconductors such as Si. Therefore, the thermal diffusion at high temperatures for doping in TMDs is inappropriate. Substitutional metal/non-metal doping during the growth process of TMDs is more favorable, which moderates the carrier density through the growth process. Numerous endeavors have done to obtain selective doping for a wide-scale synthesis process. The dopant can be selectively injected into the TMDs lattice, creating defective sites. The post-annealing after-growth process is sometimes required to activate the dopant and reconstruct the crystal structure. Generally, doping introduces impurity atoms into the TMDs structure. However, most of the time, impurity atoms are matchless to the TMDs creative lattice structure, which does not replace the original atoms of TMDs. In such a case, impurity atoms are doped into the inner region of TMDs, and many such impurity atoms disrupt the lattice structure. As previously reported by Zhang and coworkers[57] when the doping concentration of Mn in MoS_2 is higher than 2%, the lattice structure of MoS_2 gets degraded. The different metals and non-metals can be selected as dopants for TMDs; however, the

doping concentration should be optimized. Further studies are needed to investigate systematically doping into the TMDs and its associated challenges.

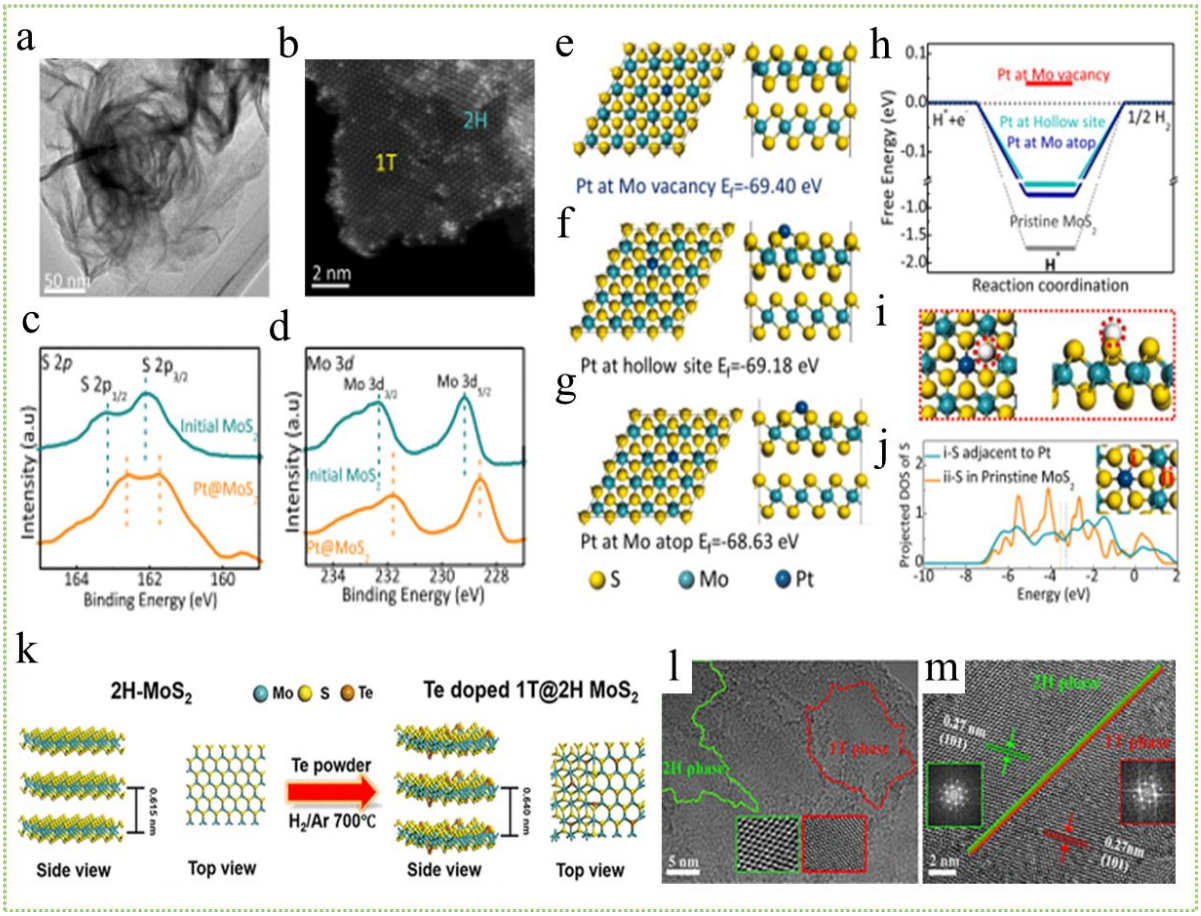

Figure 3. a, b) TEM and STEM for $Pt@MoS_2$, c, d) XPS spectra of S 2p, and Mo 3d of MoS_2 and $Pt@MoS_2$, e-g) DFT structures for Pt doping sites and equivalent formation energy. h) Free energy plots of HER at the equilibrium potential. i) Top and side view of the structure of H atom absorbed on the S atom of $Pt@MoS_2$. j) Probable p-orbital DOS of S. Reprinted with permission from ref.[48].

Copyright 2021 Elsevier. k) Schematic protocol for fabrication procedure of Te-doped 1T@2H MoS_2. l and m) atomic prearrangement of 1T (red circles) and 2H (green circles) phases and a Fourier transform image. Reprinted with permission from ref.[54]. Copyright 2019 Royal Society of Chemistry.

3.2 Surface Phase Modulation/Phase Engineering

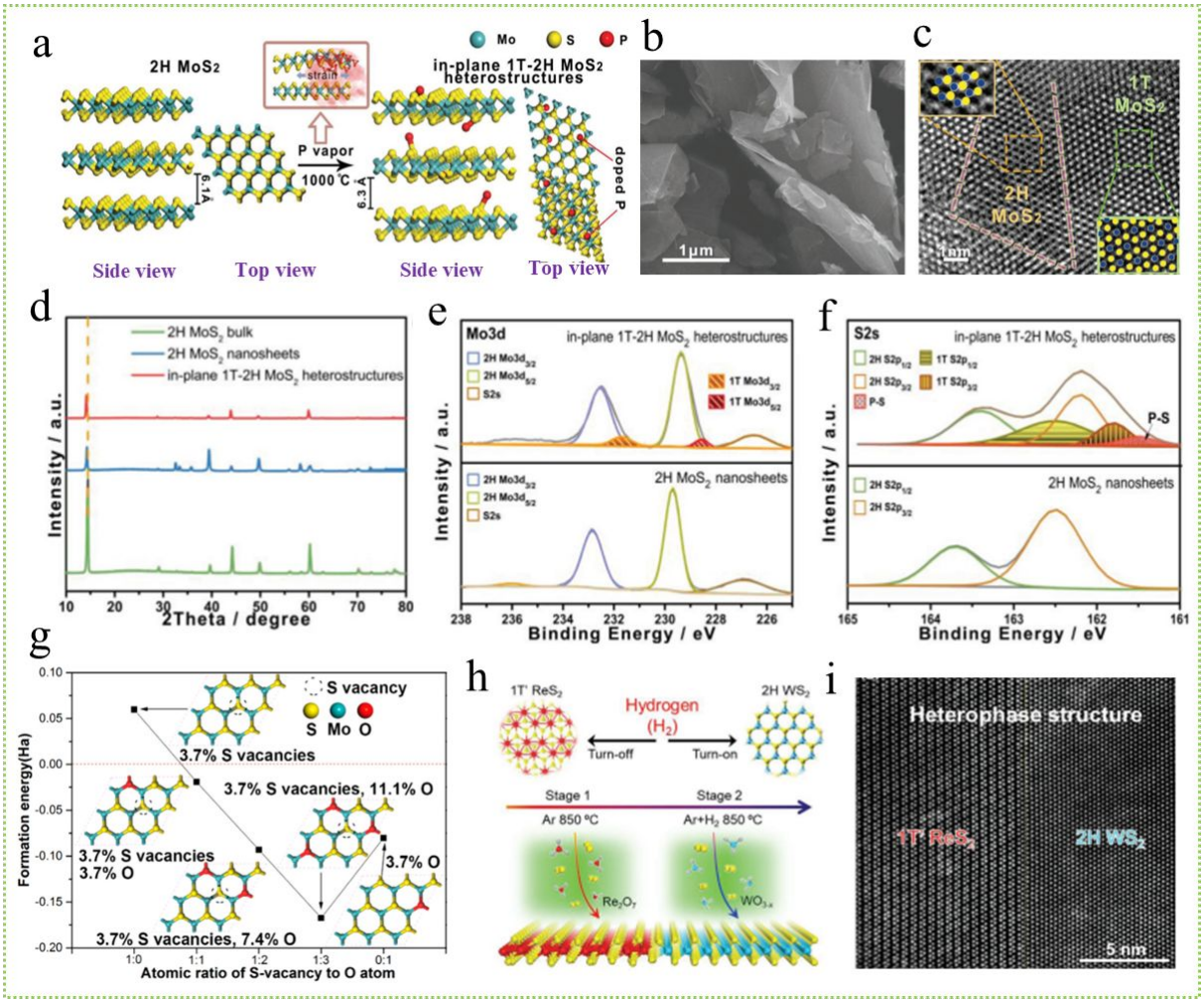

Figure 4. a) Schematic protocol for the partial phase conversion in MoS_2, b) SEM image of 1T-2H MoS_2, c) HRTEM image showing atomic arrangement for 2H and 1T phase, d) XRD pattern and XPS spectra of e) Mo 3d and f) S 2s of T-2H MoS_2. Reprinted with permission from ref.[58]. Copyright 2018 Wiley-VCH, g) plot of formation energies of 2H MoS_2 with S vacancies, O atoms and mixture of both. Reprinted from ref.[59]. Copyright 2018 American Chemical Society, h) Atomic model presenting the hydrogen-triggered synthesis of WS_2-ReS_2 and i) high-resolution ADF-STEM of heterojunction. Reprinted with permission from ref.[60]. Copyright 2020 Wiley-VCH.

Interface nanoarchitectonics through surface phase modulation is an efficient method to regulate the performance of TMDs. As discussed in the above section, TMDs are found in both metallic and semiconducting phases, namely, 1T, 2H, and 3R, based on the arrangement of M and X atoms. The phase transition in TMDs from naturally occurring 2H to 1T phase can be triggered by several routes, including chemical exfoliation, alkali metal ion intercalation, plasma treatment, electron beam irradiation, hot electron injection, etc[23]. The phase modulation in single-layer TMDs mainly depends on the number of electrons in d-orbital of metal. Modification in the filling of d-orbitals permits phase transition. Until now, there are several reports on the phase transition of group 6 TMDs including MoS_2, $MoSe_2$, WS_2, and

WSe_2[61-63]. The phase conversion in MoS_2 was first attained via alkali ion intercalation, which now became a common strategy for triggering phase conversion in other TMDs[64]. The conversion 2H to 1T phase was prompted by electron transfer from the s-orbital of alkali metal to the d-orbital of transition metal[27]. For example, Li-intercalation in 2H MoS_2 led to the construction of 1T phase MoS_2[65]. The inverse scenario of 1T to 2H phase conversion was seen in TaS_2 after Li-intercalation[66]. Kumar and coworkers[67] adopted the Li-ion exfoliation technique for 2H to 1T phase conversion in MoS_2 and got 78.6% 1T phase in the final product. The obtained material showed good catalytic activity with a Tafel slope of 53 mV/dec and an overpotential of 262 mV.

Recent studies from Wang et al.[58] demonstrated 1T-2H MoS_2 heterostructures via annealing of 2H MoS_2 in phosphorus vapors and Ar gas. Here, phosphorus was embedded into the interior of MoS_2 and inhabited the interspace in bulk MoS_2, inducing expansion of MoS_2 and, at the same time, fractional phase transfer from 2H to 1T phase. The obtained 1T-2H MoS_2 heterostructures showed a good electronic conductivity of 8620 S $m^{-1,}$ 500 times larger than bulk 2H MoS_2 (16.1 S m^{-1}). Figure 4a demonstrates a typical procedure for the fabrication of 1T-2H MoS_2, where 2H MoS_2 was treated at high temperature in red P vapor in an Ar atmosphere. The numerous nanosheets of 2H MoS_2 having lateral sizes of 500 nm to 5 μm were formed (Figure 4b). TEM image revealed two different lattice regions in plane consistent to

2H MoS_2 and 1T MoS_2, individually (Figure 4c). The most substantial diffraction peak in 2H MoS_2 corresponding to (002) was observed at 14.5 °, which shifted to 14.1 ° in 1T-2H MoS_2, indicating increased interlayer distance (Figure 4d). Analogous results were observed in XPS spectra of Mo 3d (Figure 4e) and S 2s (Figure 4f), where peaks corresponding to 1T MoS_2 appeared on decreased binding energies. Gan and coworkers[59] performed another exciting study on phase engineering of MoS_2. Here, phase conversion in MoS_2 was achieved without intercalation of guest species. This study triggered phase conversion via cyclic voltammetry by electrochemical integration of S vacancies and O intercalation into the S-Mo-S. DFT analysis revealed that the S vacancies and O doping were responsible for decreasing the band gap of MoS_2, forming 1T phase, and enhancing material conductivity. The band structures of 2H-MoS_2 (Figure 4g) were constructed because phase transition, integration of S vacancies and O-doping happened mostly on the basal plane of 2H-MoS_2. The figures showed that to form 3.7% S vacancies in 2H-MoS_2, more energy than 3.7% O atoms was required. O intercalation caused development of S vacancies as S vacancies become electronegative with the upsurge of O atoms. The authors showed that the 1T/2H MoS_2 showed much improved electrocatalytic performance compared to bare MoS_2 due to tuning of both structural and electronic properties. Furthermore, MoS_2 with 1T/2H interface exhibits excellent performance owing to metallic 1T MoS_2 in direct contact

with 2H MoS_2, thus avoiding the van der Waals gap barriers[68]. In a 2H to 1T phase transfer process, MoS_2 initially converted into a transitional 1T' state and later 1T phase. Thermodynamically, 2H MoS_2 was more stable than the other MoS_2 polymorphs. Similarly, fluorine intercalation in WS_2 persuades phase conversion from 2H phase to 1T phase[69]. Fluorination improves stability of 1T WS_2, making it more stable than the 2H WS_2.

Usually, phase conversion in exfoliated TMDs is incomplete, showing a fraction of 2H and 1T phases forming the 2H-1T hybrid phase[70]. 1T MoS_2 and 1T WS_2 show metallic characteristics, whereas the 1H-1T hybrid interfaces signify new electronic heterojunctions transversely layered structures, promising for electronic devices. Moreover, 2H to 1T phase conversion in $MoTe_2$ via laser irradiation was studied by Tan et al.[71] The Te vacancies created due to the laser irradiation offer a driving force for such phase transition. One of the most remarkable recent studies was conducted by Liu and Xu[60]. In this study, authors engineered 2H-1T′ WS_2-ReS_2 heterophase having a strident interface through hydrogen-incorporated chemical vapor deposition (Figure 4h). The heterophase structure was obtained by altering the carrier gas concentration in hydrogen. The authors showed that the growth of monolayer ReS_2 was possible using argon gas, whereas a mixture of argon and hydrogen gas formed monolayer WS_2. The sharp 2H-1T heterophase interface for WS_2-ReS_2 heterojunction

shown in Figure 4i differentiates WS_2, ReS_2, and interface sites. The electrical transport measurements across such heterophase junctions disclose solid refinement structures and polarization-sensitive photodiode properties. In our recent study, we developed 1T-2H WS_2 heterostructures through nanoarchitectonics of phosphorus mediated 2H to 1T phase transition. The obtained dual-phase 1T-2H WS_2 showed 2D transformable phase structure, enlarged interlayers and electrochemically active sites. From the theoretical analysis it was proved that the 1T WS_2 phase obtained after phosphorus doping exhibited semimetallic nature with improved electronic conductivity. Here, edge-enriched metallic phase and enhanced interlayer distance of 1T-2H WS_2 heterostructures authenticate high Na^+ ion intercalation efficiency for hybrid supercapacitor.[72] Another remarkable phase engineering study was reported by Zhai and coworkers, where reversible phase transition in WS_2 occurred[73]. The earlier reported literature on the phase transition of TMDs is mostly irreversible. The proton intercalation-deintercalation into semimetallic 1T'-WS_2 leads to reversible phase transition and distorted octahedral 1T'$_d$ – WS_2 formation. After proton deintercalation, the newly formed 1T'd – WS_2 completely transformed to the original 1T'-WS_2. The reversible phase transition phenomenon in TMDs is advantageous for transistors and memory devices.

3.3 Interface Engineering Between TMDs and Carbon-Based Materials

Carbon-based materials are widely employed as a backbone to improve the performance of TMDs, and each possesses unique characteristics and properties[74]. WS_2 monolayer has been reported as a direct semiconductor with a wide band gap of 1.98 eV[75], which is poor conductive for electron transfer. Zhang et al.[76] developed a graphene/WS_2 heterostructure to advance charge transfer features of monolayer WS_2. The electronic band structures of graphene and WS_2 were presented in Figure 5a and b. Graphene demonstrated complete metallic features with zero band gap, whereas monolayer WS_2 revealed a wide band gap. Figure 5c showed that graphene/WS_2 heterostructure demonstrated a band gap of ~1 eV, much smaller than monolayer WS_2. In heterostructure, band structure of WS_2 drifts downside, which minimizes the wide band gap of WS_2 (Figure 5d). The graphene in heterostructure efficiently improves the conductivity and donates the metallic characteristic to heterostructure, thus improving graphene/WS_2 heterostructure performance. Furthermore, Wang et al.[77] developed electronic structures of twisted bilayers of graphene/MoS_2. Authors showed that there is significant difference in band structures of twisted bilayers of graphene/MoS_2 and non-twisted one. Figure 5e and f demonstrated the structural arrangements of graphene/MoS_2 with different interlayer rotation angle. The band structure obtained for two

different rotation angles (Figure 5g) showed that the *E-k* dispersion relations are almost same for these two angles with negligible difference of 0.02 eV shift in MoS_2 energy states.

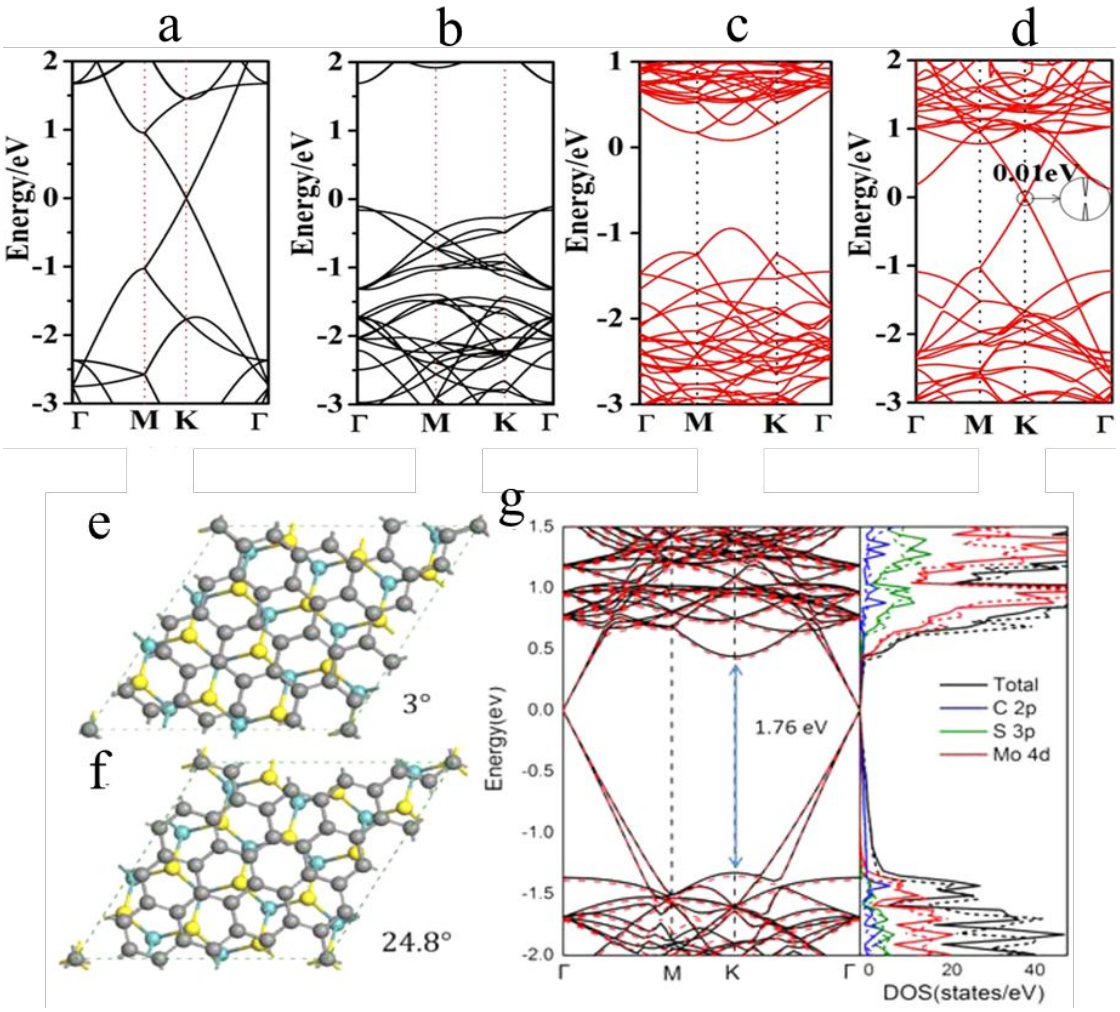

Figure 5. The electronic band structures of a) graphene, b) monolayer WS_2, c) and d) graphene/WS_2 heterostructure. Reprinted with permission from ref.[76]. Copyright 2012 Elsevier. Geometric structures of graphene/MoS_2 with different interlayer rotation angle e) $\theta = 3°$, f) $\theta =$

24.8° and g) corresponding band structures and PDOS. Reprinted from ref.[77]. Copyright 2015 American Chemical Society.

Furthermore, numerous attempts have been made to explore the geometric and electrical properties of TMDs combined with other 2D materials. Different studies on TMDs/graphene specify that such heterostructure can persuade hetero-interfacial charge transfer and improve thermodynamic stability[78]. Yu and coworkers reported another interesting structural feature of MoS_2/graphene heterostructure[79]. The synthesis procedure for self-assembled MoS_2/graphene through electrostatic attraction was shown in Figure 6a. The thermal treatment of MoS_4^{2-}/PEI/GO layers removes redundant PET and converts MoS_4^{2-} to Mos_2 and graphene oxide to graphene with stacked architecture. The low angle diffraction peaks at 7.99˚ and 16.98˚ in the XRD pattern showed extended interlayer spacings of MoS_2 and distance between MoS_2 and graphene (Figure 6b). Analogous results were obtained for Raman spectra of MoS_2/graphene (Figure 6c). The interface of MoS_2 and graphene with exclusive structural features led to edge-active sites and defects in the heterostructure, which improved electronic conductivity. Ratha et al.[80] prepared WS_2/reduced graphene oxide (RGO) through a hydrothermal route for supercapacitor. TEM and HRTEM images (Figure 6d, e) for WS_2/RGO demonstrated the even dispersal of WS_2 on RGO. Due to the

multiple chemical states of W atoms from +2 to +6, excellent energy storage performance was achieved in 1M Na_2SO_4 electrolyte. Zhang et al.[81] reported single-layer mesoporous MoS_2/carbon using SBA-15-P123 duel-template. The template avoids the addition of carbon and the use of sulfur source. The MoS_2/carbon revealed good sodium storage with a 310 mA h/g capacity at 5 A/g. Recently, bimetallic chalcogenide-tagged nitrogen-doped carbon ($NbMo_6S_8$/NC) nanosheets were demonstrated for aqueous Zn-ion capacitors. Here nitrogen doping in carbon avoided $NbMo_6S_8$ nanoflower aggregation, increased interlayer spacing and made disordered structure. The obtained $NbMo_6S_8$/NC electrode illustrated excellent electrochemical performance with a specific capacity of 167.89 mA h g^{-1} at 0.25 A g^{-1}.[82] So far, Cu_xS/carbon composite[83], WS_2/carbon[84], Co_9S_8/carbon, NiS_x/porous carbon[85], etc., has been developed, showing significant performance improvement through the interface approach.

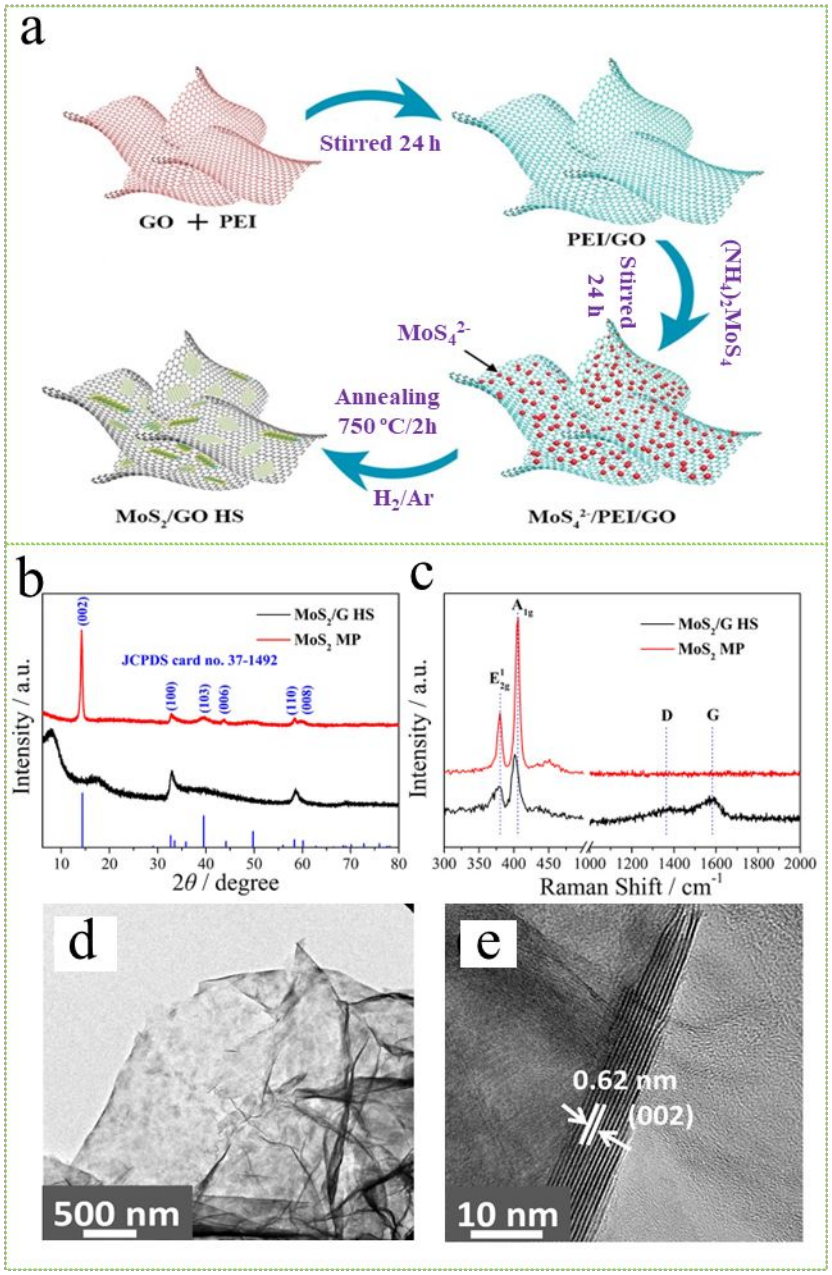

Figure 6. a) synthesis procedure for MoS_2/graphene, b) XRD pattern and Raman spectra for MoS_2/graphene. Reprinted from ref.[79]. Copyright 2020 American Chemical Society, d and e) TEM

and HRTEM images of WS_2/RGO hybrid. Reprinted from ref.[80]. Copyright 2013 American Chemical Society.

3.4 Interface Engineering between TMDs and Metal Oxides

Unlike individual 2D TMDs approaches, combining 2D and 1D materials with precise dimensions and diverse properties is expected to give multiple compensations when used in a device. Various approaches have been developed to advance the activity of TMDs, which mainly include performance improvement through electronic conductivity engineering and active site engineering. As discussed in the above section, electronic conductivity can be increased through heteroatom doping and phase transition, enabling interfacial charge transport. The active sites can be increased through surface medication. Recently, researchers enhanced the activity of 2D TMDs by developing metal sulfide/oxide heterojunction to improve the materials' performance through hybridization synergistic effect. For example, Hu et al.[86] developed high-performance MoS_2/metal oxide heterostructures through modulating interface electronic structure. The electronic structures of MoS_2/Ni_2O_3H, MoS_2/Co_3O_4, and MoS_2/Fe_2O_3 were attained from the density functional theory

(DFT) calculations (Figure 7a-c). The electron distribution was mainly observed on the interface near the Fermi level (E_f) for MoS_2/Ni_2O_3H. The apparent strain was observed near the interface, leading to structure distortion, and the most electroactive sites were transition metals near the interface. Figure 7d-g demonstrated that high electrochemically active sites were at the TMDs/metal oxide interface region, suitable for the hydrogen evolution activity. From the sensitivity of 3d-band in different transition oxides, Ni-3d of Ni_2O_3H towards the interface is highly stimulated to accomplish fast electron transfer. Wang and coworkers[87] prepared WS_2 nanotubes by sulfurization of WO_3 nanowires. The HRTEM images in Figure 7h and i demonstrated three-layer walled and six-layer walled WS_2 nanotubes, respectively, with the same outer diameter of 10 nm. It was clearly seen that a longer sulfurization time increased the number of WS_2 layers. Thus, WO_3/WS_2 interface structure was easily obtained by controlling the preparation conditions.

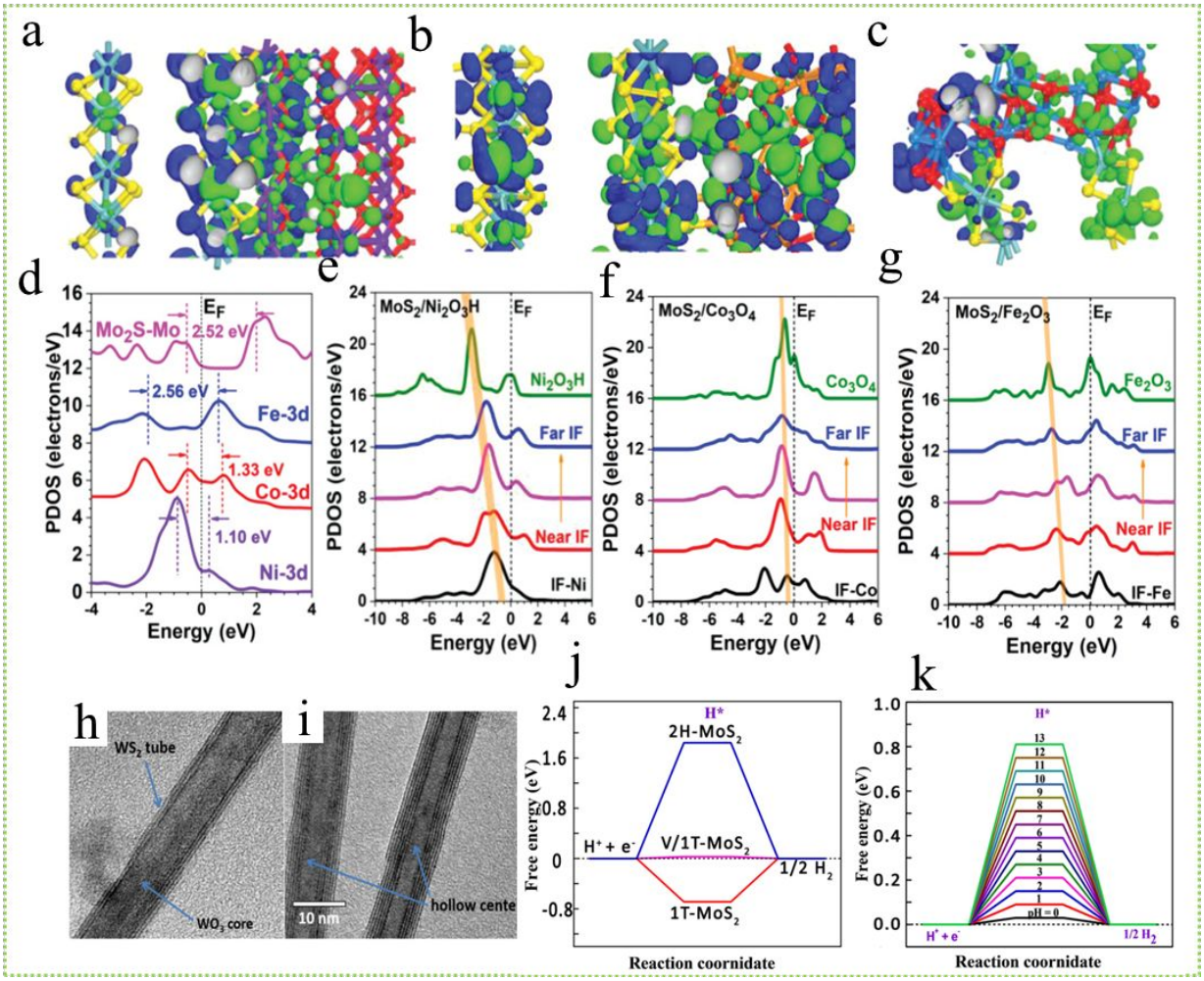

Figure 7. The contour plots for bonding and anti-bonding orbitals near the fermi level for a) MoS_2/Ni_2O_3H, b) MoS_2/Co_3O_4, and c) MoS_2/Fe_2O_3. d) PDOSs of 3d bands of MoS_2/Ni_2O_3H, MoS_2/Co_3O_4, and MoS_2/Fe_2O_3. e) Site-dependent 3d-band of Ni in MoS_2/Ni_2O_3H. f) Site-dependent 3d-band of Co in MoS_2/Co_3O_4. g) Site-dependent 3d-band of Fe in MoS_2/Fe_2O_3. Reprinted with permission from ref.[86]. Copyright 2020 Wiley-VCH. HRTEM images for h) three-layer and i) six-layer WS_2 nanotubes and inside WO_3 core. Reprinted with permission from ref.[87].

Copyright 2016 Springer-Nature. j) Gibbs free energy diagram for hydrogen evolution of 2H MoS_2, 1T MoS_2 and V doped 1T MoS_2 and k) Gibbs free energy of V doped 1T MoS_2 in a pH range of 0 to 13. Reprinted with permission from ref.[88]. Copyright 2021 Elsevier.

Li and co-workers[88] developed vanadium doped 1T MoS_2 nanosheets directly on a carbon paper. Here, the direct growth of material on current collector empowers good integration and decreases the resistance. The hydrazine molecules form precursors intercalated into MoS_2 and acted as Lewis base, provided additional electron to maintained 1T phase of MoS_2. Theoretical calculations proved that the vanadium doped 1T MoS_2 offered nearly zero Gibbs free energy, which achieved best hydrogen adsorption. Figure 7j showed the calculated Gibbs free energy diagram for hydrogen evolution activity of 2H MoS_2, 1T MoS_2 and vanadium doped 1T MoS_2, which proved that vanadium doped 1T MoS_2 had lowest ΔG_H value of 0.03 eV and better performance. The Gibbs free energy of vanadium doped 1T MoS_2 in full pH range was shown in Figure 7k. Jung and Choudhari[89] developed a 1D/2D WO_3/WS_2 core-shell interface structure directly on the W foil substrate through an unprompted oxidation/sulfurization process. Similarly, $WS_2@NiCo_2O_4$[90], Co_3O_4/MoS_2[91] TMDs/metal oxide heterostructures have been developed with exciting interface properties. Thus, the overall results indicate that composites of TMDs with metal oxides enhance

the conductivity of material, facilitating rapid charge carrier transport, which may be further employed for potential applications.

4 Conclusions

The recent advancement in interface and phase engineering of 2D TMDs for tuning their properties to achieve high electronic conductivity and superior interfacial characteristics has been reviewed. Different types of interfaces in TMDs-based materials arising from intercalation of guest ions, phase modulation, TMDs/carbon, and TMDs/metal oxide contact, which can be adequately engineered through interface engineering strategies. The phase transition via surface charge doping at the TMDs interface has been considered an efficient way to modify the charge carrier density, which deliberately impacts the electronic properties and performance of device. The TMDs/metal interface obtained via heteroatom doping i.e., intrinsic impurity atoms present at TMDs interface, enables charge carrier transport in TMDs. Furthermore, partial phase conversion in TMDs from naturally occurring 2H semiconducting to 1T metallic phase showed superior structural advantages, improved electrical conductivity, and highly exposed basal and edge active sites that are advantageous for catalysis and energy applications. For energy storage devices such as supercapacitors and rechargeable batteries, interface engineering improves the charge storage

efficiency through their expanded interlayers. As an HER electrocatalysis, this strategy lowers the Gibbs free energy, enables fast proton/electron adsorption and hydrogen release, beneficial for good HER activity.

Moreover, interface nanoarchitectonics analyses[92] different defects present in the lattice structure of TMCs, including intercalated impurities, grain boundaries, vacancies, and phase conversion and their consequences on the electronic features of TMCs. Proper interface engineering can remarkably enable charge carrier density, creating active heteroatom intercalation and dropping the contact resistance in electronic devices. Furthermore, implementation of electronic as well as energy storage and conversion devices based on 2D TMDs necessitates controlled interface engineering to further improve their charge carrier density and device performance. This strategy can be further prolonged to produce TMDs with dual-phase structures, interfaces, and defects and sheds light on the expansion of future 2D TMDs.

Even though there has been much advances in the development of phase modulated and interlayer expanded TMDs and their wide applications in various fields, still there are many challenges. It is tough to synthesize TMDs in a single step with controlled size, layer number, interlayer distance phase composition, number of guest species to obtained optimal material and

performance are yet to be industrialized. The relation between quantities, type of guess ions and interlayer distance and their device performance are not yet well-known. The intercalation sites of guest dopants and their intercalation with TMDs need to be understood.

Author Information

Corresponding Author

* **Prof. Katsuhiko Ariga** - *Research Center for Materials Nanoarchitectonics, National Institute for Materials Science (NIMS), 1-1 Namiki, Tsukuba 305-0044, Japan; Email:* ARIGA.katsuhiko@nims.go.jp. ***Dr. Pragati A. Shinde** - *Research Center for Materials Nanoarchitectonics, National Institute for Materials Science (NIMS), 1-1 Namiki, Tsukuba 305-0044, Japan; Email:* SHINDE.PragatiAnkush@nims.go.jp.

Notes

The authors declare no competing financial interest.

Acknowledgment

This work is supported by the Japan Society for the Promotion of Science (JSPS) KAKENHI Grant Number JP22F22368.

References

1. Luo, B.; Liu, G.; Wang, L., Recent advances in 2D materials for photocatalysis. *Nanoscale* **2016,** *8* (13), 6904-6920.

2. Schaibley, J. R.; Yu, H.; Clark, G.; Rivera, P.; Ross, J. S.; Seyler, K. L.; Yao, W.; Xu, X., Valleytronics in 2D materials. *Nature Reviews Materials* **2016,** *1* (11), 1-15.

3. Wang, F.; Wang, Z.; Yin, L.; Cheng, R.; Wang, J.; Wen, Y.; Shifa, T. A.; Wang, F.; Zhang, Y.; Zhan, X.; He, J., 2D library beyond graphene and transition metal dichalcogenides: a focus on photodetection. *Chemical Society Reviews* **2018,** *47* (16), 6296-6341.

4. Shinde, P. A.; Olabi, A. G.; Chodankar, N. R.; Patil, S. J.; Hwang, S.-K.; Abdelkareem, M. A., Realizing superior redox kinetics of metal-metal carbides/carbon coordination supported heterointerface for stable solid-state hybrid supercapacitor. *Chemical Engineering Journal* **2023,** *454*, 140246.

5. Wang, S.; Robertson, A.; Warner, J. H., Atomic structure of defects and dopants in 2D layered transition metal dichalcogenides. *Chemical Society Reviews* **2018,** *47* (17), 6764-6794.

6. Wang, H.; Yuan, H.; Sae Hong, S.; Li, Y.; Cui, Y., Physical and chemical tuning of two-dimensional transition metal dichalcogenides. *Chemical Society Reviews* **2015,** *44* (9), 2664-2680.

7. Shinde, P. A.; Chodankar, N. R.; Abdelkareem, M. A.; Patil, S. J.; Han, Y.-K.; Elsaid, K.; Olabi, A. G., All Transition Metal Selenide Composed High-Energy Solid-State Hybrid Supercapacitor. *Small* **2022,** *18* (20), 2200248.

8. Han, G. H.; Duong, D. L.; Keum, D. H.; Yun, S. J.; Lee, Y. H., van der Waals Metallic Transition Metal Dichalcogenides. *Chemical Reviews* **2018,** *118* (13), 6297-6336.

9. Lim, C. S.; Tan, S. M.; Sofer, Z.; Pumera, M., Impact Electrochemistry of Layered Transition Metal Dichalcogenides. *ACS Nano* **2015,** *9* (8), 8474-8483.

10. Qian, Q.; Zhang, Z.; Chen, K. J., In Situ Resonant Raman Spectroscopy to Monitor the Surface Functionalization of MoS2 and WSe2 for High-k Integration: A First-Principles Study. *Langmuir* **2018,** *34* (8), 2882-2889.

11. Ishii, M.; Yamashita, Y.; Watanabe, S.; Ariga, K.; Takeya, J., Doping of molecular semiconductors through proton-coupled electron transfer. *Nature* **2023,** *622* (7982), 285-291.

12. Patil, S. J.; Chodankar, N. R.; Hwang, S.-K.; Shinde, P. A.; Rama Raju, G. S.; Ranjith, K. S.; Karekar, S. V.; Huh, Y.-S.; Han, Y.-K., Two-dimensional nanosheets of bimetallic chalcogenide-tagged nitrogen-doped carbon as a cathode for high-performance and durable zinc-ion capacitors. *Journal of Materials Chemistry A* **2023,** *11* (10), 5112-5126.

13. Ho, W.; Yu, J. C.; Lin, J.; Yu, J.; Li, P., Preparation and Photocatalytic Behavior of MoS2 and WS2 Nanocluster Sensitized TiO2. *Langmuir* **2004,** *20* (14), 5865-5869.

14. Liang, C.; Sun, K.; Chen, M.; Xu, P., Crystal-Phase Engineering of Two-Dimensional Transition-Metal Dichalcogenides for Surface-Enhanced Raman Scattering: A Perspective. *Langmuir* **2023,** *39* (34), 11946-11953.

15. Patil, S. J.; Chodankar, N. R.; Hwang, S.-K.; Shinde, P. A.; Seeta Rama Raju, G.; Shanmugam Ranjith, K.; Huh, Y. S.; Han, Y.-K., Co-metal–organic framework derived CoSe2@MoSe2 core–shell structure on carbon cloth as an efficient bifunctional catalyst for overall water splitting. *Chemical Engineering Journal* **2022,** *429*, 132379.

16. Tedstone, A. A.; Lewis, D. J.; O'Brien, P., Synthesis, Properties, and Applications of Transition Metal-Doped Layered Transition Metal Dichalcogenides. *Chemistry of Materials* **2016,** *28* (7), 1965-1974.

17. Pi, L.; Li, L.; Liu, K.; Zhang, Q.; Li, H.; Zhai, T., Recent Progress on 2D Noble-Transition-Metal Dichalcogenides. *Advanced Functional Materials* **2019,** *29* (51), 1904932.

18. Wei, Z.; Li, B.; Xia, C.; Cui, Y.; He, J.; Xia, J.-B.; Li, J., Various Structures of 2D Transition-Metal Dichalcogenides and Their Applications. *Small Methods* **2018,** *2* (11), 1800094.

19. Wu, X.; Zhang, H.; Zhang, J.; Lou, X. W., Recent Advances on Transition Metal Dichalcogenides for Electrochemical Energy Conversion. *Advanced Materials* **2021,** *33* (38), 2008376.

20. Khan, M. F.; Ahmed, F.; Rehman, S.; Akhtar, I.; Rehman, M. A.; Shinde, P. A.; Khan, K.; Kim, D.-K.; Eom, J.; Lipsanen, H., High performance complementary WS 2 devices with hybrid Gr/Ni contacts. *Nanoscale* **2020,** *12* (41), 21280-21290.

21. Li, H.; Wu, J.; Yin, Z.; Zhang, H., Preparation and applications of mechanically exfoliated single-layer and multilayer MoS2 and WSe2 nanosheets. *Accounts of chemical research* **2014,** *47* (4), 1067-1075.

22. Li, Y.; Wang, H.; Xie, L.; Liang, Y.; Hong, G.; Dai, H., MoS2 Nanoparticles Grown on Graphene: An Advanced Catalyst for the Hydrogen Evolution Reaction. *Journal of the American Chemical Society* **2011,** *133* (19), 7296-7299.

23. Voiry, D.; Mohite, A.; Chhowalla, M., Phase engineering of transition metal dichalcogenides. *Chemical Society Reviews* **2015,** *44* (9), 2702-2712.

24. Zhao, Y.; Xu, K.; Pan, F.; Zhou, C.; Zhou, F.; Chai, Y., Doping, Contact and Interface Engineering of Two-Dimensional Layered Transition Metal Dichalcogenides Transistors. *Advanced Functional Materials* **2017,** *27* (19), 1603484.

25. Rohaizad, N.; Mayorga-Martinez, C. C.; Sofer, Z.; Pumera, M., 1T-Phase Transition Metal Dichalcogenides (MoS2, MoSe2, WS2, and WSe2) with Fast Heterogeneous Electron Transfer: Application on Second-Generation Enzyme-Based Biosensor. *ACS Applied Materials & Interfaces* **2017,** *9* (46), 40697-40706.

26. Chen, B.; Chao, D.; Liu, E.; Jaroniec, M.; Zhao, N.; Qiao, S.-Z., Transition metal dichalcogenides for alkali metal ion batteries: engineering strategies at the atomic level. *Energy & Environmental Science* **2020,** *13* (4), 1096-1131.

27. Chhowalla, M.; Shin, H. S.; Eda, G.; Li, L.-J.; Loh, K. P.; Zhang, H., The chemistry of two-dimensional layered transition metal dichalcogenide nanosheets. *Nature Chemistry* **2013,** *5* (4), 263-275.

28. Huang, X.; Zeng, Z.; Zhang, H., Metal dichalcogenide nanosheets: preparation, properties and applications. *Chemical Society Reviews* **2013,** *42* (5), 1934-1946.

29. Qian, X.; Liu, J.; Fu, L.; Li, J., Quantum spin Hall effect in two-dimensional transition metal dichalcogenides. *Science* **2014,** *346* (6215), 1344-1347.

30. Wang, Q. H.; Kalantar-Zadeh, K.; Kis, A.; Coleman, J. N.; Strano, M. S., Electronics and optoelectronics of two-dimensional transition metal dichalcogenides. *Nature Nanotechnology* **2012,** *7* (11), 699-712.

31. Bhimanapati, G. R.; Lin, Z.; Meunier, V.; Jung, Y.; Cha, J.; Das, S.; Xiao, D.; Son, Y.; Strano, M. S.; Cooper, V. R.; Liang, L.; Louie, S. G.; Ringe, E.; Zhou, W.; Kim, S. S.; Naik, R. R.; Sumpter, B. G.; Terrones, H.; Xia, F.; Wang, Y.; Zhu, J.; Akinwande, D.; Alem, N.; Schuller, J. A.; Schaak, R. E.; Terrones, M.; Robinson, J. A., Recent Advances in Two-Dimensional Materials beyond Graphene. *ACS Nano* **2015,** *9* (12), 11509-11539.

32. Samadi, M.; Sarikhani, N.; Zirak, M.; Zhang, H.; Zhang, H.-L.; Moshfegh, A. Z., Group 6 transition metal dichalcogenide nanomaterials: synthesis, applications and future perspectives. *Nanoscale Horizons* **2018,** *3* (2), 90-204.

33. Tang, Q.; Jiang, D.-e., Stabilization and Band-Gap Tuning of the 1T-MoS_2 Monolayer by Covalent Functionalization. *Chemistry of Materials* **2015,** *27* (10), 3743-3748.

34. Fu, W.; John, M.; Maddumapatabandi, T. D.; Bussolotti, F.; Yau, Y. S.; Lin, M.; Johnson Goh, K. E., Toward Edge Engineering of Two-Dimensional Layered Transition-Metal Dichalcogenides by Chemical Vapor Deposition. *ACS Nano* **2023,** *17* (17), 16348-16368.

35. Cho, K.; Pak, J.; Chung, S.; Lee, T., Recent Advances in Interface Engineering of Transition-Metal Dichalcogenides with Organic Molecules and Polymers. *ACS Nano* **2019,** *13* (9), 9713-9734.

36. Lukowski, M. A.; Daniel, A. S.; Meng, F.; Forticaux, A.; Li, L.; Jin, S., Enhanced Hydrogen Evolution Catalysis from Chemically Exfoliated Metallic MoS2 Nanosheets. *Journal of the American Chemical Society* **2013,** *135* (28), 10274-10277.

37. Liu, Q.; Li, X.; Xiao, Z.; Zhou, Y.; Chen, H.; Khalil, A.; Xiang, T.; Xu, J.; Chu, W.; Wu, X.; Yang, J.; Wang, C.; Xiong, Y.; Jin, C.; Ajayan, P. M.; Song, L., Stable Metallic 1T-WS2 Nanoribbons Intercalated with Ammonia Ions: The Correlation between Structure and Electrical/Optical Properties. *Advanced Materials* **2015,** *27* (33), 4837-4844.

38. Choi, W.; Choudhary, N.; Han, G. H.; Park, J.; Akinwande, D.; Lee, Y. H., Recent development of two-dimensional transition metal dichalcogenides and their applications. *Materials Today* **2017,** *20* (3), 116-130.

39. Komsa, H.-P.; Kotakoski, J.; Kurasch, S.; Lehtinen, O.; Kaiser, U.; Krasheninnikov, A. V., Two-dimensional transition metal dichalcogenides under electron irradiation: defect production and doping. *Physical review letters* **2012,** *109* (3), 035503.

40. Zhang, T.; Fujisawa, K.; Zhang, F.; Liu, M.; Lucking, M. C.; Gontijo, R. N.; Lei, Y.; Liu, H.; Crust, K.; Granzier-Nakajima, T., Universal in situ substitutional doping of transition metal dichalcogenides by liquid-phase precursor-assisted synthesis. *ACS nano* **2020,** *14* (4), 4326-4335.

41. Kang, M.; Lin, C.; Yang, H.; Guo, Y.; Liu, L.; Xue, T.; Liu, Y.; Gong, Y.; Zhao, Z.; Zhai, T., Proximity enhanced hydrogen evolution reactivity of substitutional doped monolayer WS2. *ACS Applied Materials & Interfaces* **2021,** *13* (16), 19406-19413.

42. Kumar, Y. A.; Al-Asbahi, B. A.; Pallavolu, M. R.; Rao, S. S.; Nallapureddy, R. R.; Ramakrishna, S., Multiple structural defects in poor crystalline nickel-doped tungsten disulfide nanorods remarkably enhance supercapacitive performance. *International Journal of Energy Research* **2022,** *46* (10), 14227-14239.

43. Bello, I. T.; Oladipo, A. O.; Adedokun, O.; Dhlamini, S. M., Recent advances on the preparation and electrochemical analysis of MoS2-based materials for supercapacitor applications: A mini-review. *Materials Today Communications* **2020,** *25*, 101664.

44. Tan, X.; Zhao, D.; Sun, Y.; Duan, Z.; Wang, X.; Wu, X., Co-doped MoS2 nanosheet: a stable and pH-universal electrocatalyst for an efficient hydrogen evolution reaction. *CrystEngComm* **2022,** *24* (38), 6696-6704.

45. Prakash, K.; Harish, S.; Kamalakannan, S.; Logu, T.; Shimomura, M.; Archana, J.; Navaneethan, M., Perspective on ultrathin layered Ni-doped MoS2 hybrid nanostructures for the enhancement of electrochemical properties in supercapacitors. *Journal of Energy Chemistry* **2023,** *80*, 335-349.

46. Luo, Z.; Ouyang, Y.; Zhang, H.; Xiao, M.; Ge, J.; Jiang, Z.; Wang, J.; Tang, D.; Cao, X.; Liu, C.; Xing, W., Chemically activating MoS2 via spontaneous atomic palladium interfacial doping towards efficient hydrogen evolution. *Nature Communications* **2018,** *9* (1), 2120.

47. Guruprasad, K.; Maiyalagan, T.; Shanmugam, S., Phosphorus Doped MoS2 Nanosheet Promoted with Nitrogen, Sulfur Dual Doped Reduced Graphene Oxide as an Effective

Electrocatalyst for Hydrogen Evolution Reaction. *ACS Applied Energy Materials* **2019,** *2* (9), 6184-6194.

48. Li, Y.; Gu, Q.; Johannessen, B.; Zheng, Z.; Li, C.; Luo, Y.; Zhang, Z.; Zhang, Q.; Fan, H.; Luo, W., Synergistic Pt doping and phase conversion engineering in two-dimensional MoS2 for efficient hydrogen evolution. *Nano Energy* **2021,** *84*, 105898.

49. Yin, Y.; Han, J.; Zhang, Y.; Zhang, X.; Xu, P.; Yuan, Q.; Samad, L.; Wang, X.; Wang, Y.; Zhang, Z.; Zhang, P.; Cao, X.; Song, B.; Jin, S., Contributions of Phase, Sulfur Vacancies, and Edges to the Hydrogen Evolution Reaction Catalytic Activity of Porous Molybdenum Disulfide Nanosheets. *Journal of the American Chemical Society* **2016,** *138* (25), 7965-7972.

50. Laskar, M. R.; Nath, D. N.; Ma, L.; Lee, E. W.; Lee, C. H.; Kent, T.; Yang, Z.; Mishra, R.; Roldan, M. A.; Idrobo, J.-C., p-type doping of MoS2 thin films using Nb. *Applied Physics Letters* **2014,** *104* (9).

51. McDonnell, S.; Addou, R.; Buie, C.; Wallace, R. M.; Hinkle, C. L., Defect-dominated doping and contact resistance in MoS2. *ACS nano* **2014,** *8* (3), 2880-2888.

52. Bian, L.; Gao, W.; Sun, J.; Han, M.; Li, F.; Gao, Z.; Shu, L.; Han, N.; Yang, Z. x.; Song, A., Phosphorus-Doped MoS2 Nanosheets Supported on Carbon Cloths as Efficient Hydrogen-Generation Electrocatalysts. *ChemCatChem* **2018,** *10* (7), 1571-1577.

53. Ye, R.; del Angel-Vicente, P.; Liu, Y.; Arellano-Jimenez, M. J.; Peng, Z.; Wang, T.; Li, Y.; Yakobson, B. I.; Wei, S. H.; Yacaman, M. J., High-performance hydrogen evolution from MoS2 (1–x) P x solid solution. *Advanced Materials* **2016,** *28* (7), 1427-1432.

54. Li, W.; Shen, Y.; Xiao, X.; An, C.; Wei, G.; Wang, Y.; Wang, J.; Wu, Y.; An, C., Simple Te-Thermal Converting 2H to 1T@2H MoS2 Homojunctions with Enhanced Supercapacitor Performance. *ACS Applied Energy Materials* **2019,** *2* (11), 8337-8344.

55. Liu, P.; Zhu, J.; Zhang, J.; Xi, P.; Tao, K.; Gao, D.; Xue, D., P Dopants Triggered New Basal Plane Active Sites and Enlarged Interlayer Spacing in MoS2 Nanosheets toward Electrocatalytic Hydrogen Evolution. *ACS Energy Letters* **2017,** *2* (4), 745-752.

56. Shi, X.; Fields, M.; Park, J.; McEnaney, J. M.; Yan, H.; Zhang, Y.; Tsai, C.; Jaramillo, T. F.; Sinclair, R.; Nørskov, J. K.; Zheng, X., Rapid flame doping of Co to WS2 for efficient hydrogen evolution. *Energy & Environmental Science* **2018,** *11* (8), 2270-2277.

57. Zhang, K.; Feng, S.; Wang, J.; Azcatl, A.; Lu, N.; Addou, R.; Wang, N.; Zhou, C.; Lerach, J.; Bojan, V.; Kim, M. J.; Chen, L.-Q.; Wallace, R. M.; Terrones, M.; Zhu, J.; Robinson, J. A., Manganese Doping of Monolayer MoS2: The Substrate Is Critical. *Nano Letters* **2015,** *15* (10), 6586-6591.

58. Wang, S.; Zhang, D.; Li, B.; Zhang, C.; Du, Z.; Yin, H.; Bi, X.; Yang, S., Ultrastable In-Plane 1T–2H MoS2 Heterostructures for Enhanced Hydrogen Evolution Reaction. *Advanced Energy Materials* **2018,** *8* (25), 1801345.

59. Gan, X.; Lee, L. Y. S.; Wong, K.-y.; Lo, T. W.; Ho, K. H.; Lei, D. Y.; Zhao, H., 2H/1T Phase Transition of Multilayer MoS2 by Electrochemical Incorporation of S Vacancies. *ACS Applied Energy Materials* **2018,** *1* (9), 4754-4765.

60. Liu, D.; Hong, J.; Li, X.; Zhou, X.; Jin, B.; Cui, Q.; Chen, J.; Feng, Q.; Xu, C.; Zhai, T., Synthesis of 2H-1T′ WS2-ReS2 heterophase structures with atomically sharp interface via hydrogen-triggered one-pot growth. *Advanced Functional Materials* **2020,** *30* (16), 1910169.

61. Kan, M.; Wang, J.; Li, X.; Zhang, S.; Li, Y.; Kawazoe, Y.; Sun, Q.; Jena, P., Structures and phase transition of a MoS2 monolayer. *The Journal of Physical Chemistry C* **2014,** *118* (3), 1515-1522.

62. Wang, H.; Wang, X.; Wang, L.; Wang, J.; Jiang, D.; Li, G.; Zhang, Y.; Zhong, H.; Jiang, Y., Phase transition mechanism and electrochemical properties of nanocrystalline MoSe2 as anode materials for the high performance lithium-ion battery. *The Journal of Physical Chemistry C* **2015,** *119* (19), 10197-10205.

63. Rohaizad, N.; Mayorga-Martinez, C. C.; Sofer, Z. k.; Pumera, M., 1T-phase transition metal dichalcogenides (MoS2, MoSe2, WS2, and WSe2) with fast heterogeneous electron transfer: application on second-generation enzyme-based biosensor. *ACS applied materials & interfaces* **2017,** *9* (46), 40697-40706.

64. Py, M.; Haering, R., Structural destabilization induced by lithium intercalation in MoS2 and related compounds. *Canadian Journal of Physics* **1983,** *61* (1), 76-84.

65. Nasr Esfahani, D.; Leenaerts, O.; Sahin, H.; Partoens, B.; Peeters, F., Structural transitions in monolayer MoS2 by lithium adsorption. *The Journal of Physical Chemistry C* **2015,** *119* (19), 10602-10609.

66. Ganal, P.; Olberding, W.; Butz, T.; Ouvrard, G., Soft chemistry induced host metal coordination change from octahedral to trigonal prismatic in 1T-TaS2. *Solid State Ionics* **1993,** *59* (3-4), 313-319.

67. Venkateshwaran, S.; Senthil Kumar, S. M., Provoking Metallic 1T Phase Conversion of 2H-MoS2 via an Effectual Solvothermal Route for Electrocatalytic Water Reduction in Acid. *ACS Sustainable Chemistry & Engineering* **2022,** *10* (16), 5258-5267.

68. Zong, B.; Li, Q.; Chen, X.; Liu, C.; Li, L.; Ruan, J.; Mao, S., Highly Enhanced Gas Sensing Performance Using a 1T/2H Heterophase MoS2 Field-Effect Transistor at Room Temperature. *ACS Applied Materials & Interfaces* **2020,** *12* (45), 50610-50618.

69. Radhakrishnan, S.; Das, D.; Deng, L.; Sudeep, P. M.; Colas, G.; de los Reyes, C. A.; Yazdi, S.; Chu, C. W.; Martí, A. A.; Tiwary, C. S.; Filleter, T.; Singh, A. K.; Ajayan, P. M., An Insight into the Phase Transformation of WS2 upon Fluorination. *Advanced Materials* **2018,** *30* (44), 1803366.

70. Eda, G.; Fujita, T.; Yamaguchi, H.; Voiry, D.; Chen, M.; Chhowalla, M., Coherent atomic and electronic heterostructures of single-layer MoS2. *ACS nano* **2012,** *6* (8), 7311-7317.

71. Tan, Y.; Luo, F.; Zhu, M.; Xu, X.; Ye, Y.; Li, B.; Wang, G.; Luo, W.; Zheng, X.; Wu, N.; Yu, Y.; Qin, S.; Zhang, X.-A., Controllable 2H-to-1T′ phase transition in few-layer MoTe2. *Nanoscale* **2018,** *10* (42), 19964-19971.

72. Shinde, P. A.; Chodankar, N. R.; Kim, H.-J.; Abdelkareem, M. A.; Ghaferi, A. A.; Han, Y.-K.; Olabi, A. G.; Ariga, K., Ultrastable 1T-2H WS2 Heterostructures by Nanoarchitectonics of Phosphorus-Triggered Phase Transition for Hybrid Supercapacitors. *ACS Energy Letters* **2023,** *8* (10), 4474-4487.

73. Zhai, W.; Qi, J.; Xu, C.; Chen, B.; Li, Z.; Wang, Y.; Zhai, L.; Yao, Y.; Li, S.; Zhang, Q.; Ge, Y.; Chi, B.; Ren, Y.; Huang, Z.; Lai, Z.; Gu, L.; Zhu, Y.; He, Q.; Zhang, H., Reversible Semimetal–Semiconductor Transition of Unconventional-Phase WS2 Nanosheets. *Journal of the American Chemical Society* **2023,** *145* (24), 13444-13451.

74. Ren, Y.; Zeng, D.; Ong, W.-J., Interfacial engineering of graphitic carbon nitride (g-C3N4)-based metal sulfide heterojunction photocatalysts for energy conversion: A review. *Chinese Journal of Catalysis* **2019,** *40* (3), 289-319.

75. Wang, L.; Kutana, A.; Yakobson, B. I., Many-body and spin-orbit effects on direct-indirect band gap transition of strained monolayer MoS2 and WS2. *Annalen der Physik* **2014,** *526* (9-10), L7-L12.

76. Zhang, M.; Tang, C.; Cheng, W.; Fu, L., The first-principles study on the performance of the graphene/WS2 heterostructure as an anode material of Li-ion battery. *Journal of Alloys and Compounds* **2021,** *855*, 157432.

77. Wang, Z.; Chen, Q.; Wang, J., Electronic structure of twisted bilayers of graphene/MoS2 and MoS2/MoS2. *The Journal of Physical Chemistry C* **2015,** *119* (9), 4752-4758.

78. Zhang, K.; Jin, B.; Gao, Y.; Zhang, S.; Shin, H.; Zeng, H.; Park, J. H., Aligned heterointerface-induced 1T-MoS2 monolayer with near-ideal gibbs free for stable hydrogen evolution reaction. *Small* **2019,** *15* (8), 1804903.

79. Yu, X.; Zhao, G.; Gong, S.; Liu, C.; Wu, C.; Lyu, P.; Maurin, G.; Zhang, N., Design of MoS2/Graphene van der Waals Heterostructure as Highly Efficient and Stable Electrocatalyst for Hydrogen Evolution in Acidic and Alkaline Media. *ACS Applied Materials & Interfaces* **2020,** *12* (22), 24777-24785.

80. Ratha, S.; Rout, C. S., Supercapacitor Electrodes Based on Layered Tungsten Disulfide-Reduced Graphene Oxide Hybrids Synthesized by a Facile Hydrothermal Method. *ACS Applied Materials & Interfaces* **2013,** *5* (21), 11427-11433.

81. Zhang, X.; Weng, W.; Gu, H.; Hong, Z.; Xiao, W.; Wang, F.; Li, W.; Gu, D., Versatile Preparation of Mesoporous Single-Layered Transition-Metal Sulfide/Carbon Composites for Enhanced Sodium Storage. *Advanced Materials* **2022,** *34* (2), 2104427.

82. Patil, S. J.; Chodankar, N. R.; Hwang, S.-K.; Shinde, P. A.; Raju, G. S. R.; Ranjith, K. S.; Karekar, S. V.; Huh, Y.-S.; Han, Y.-K., Two-dimensional nanosheets of bimetallic chalcogenide-tagged nitrogen-doped carbon as a cathode for high-performance and durable zinc-ion capacitors. *Journal of Materials Chemistry A* **2023,** *11* (10), 5112-5126.

83. Foley, S.; Geaney, H.; Bree, G.; Stokes, K.; Connolly, S.; Zaworotko, M. J.; Ryan, K. M., Copper Sulfide (CuxS) Nanowire-in-Carbon Composites Formed from Direct Sulfurization of the Metal-Organic Framework HKUST-1 and Their Use as Li-Ion Battery Cathodes. *Advanced Functional Materials* **2018,** *28* (19), 1800587.

84. Shrivastav, V.; Sundriyal, S.; Shrivastav, V.; Tiwari, U. K.; Deep, A., WS2/Carbon Composites and Nanoporous Carbon Structures Derived from Zeolitic Imidazole Framework for Asymmetrical Supercapacitors. *Energy & Fuels* **2021,** *35* (18), 15133-15142.

85. Li, S.; He, W.; Liu, B.; Cui, J.; Wang, X.; Peng, D.-L.; Liu, B.; Qu, B., One-step construction of three-dimensional nickel sulfide-embedded carbon matrix for sodium-ion batteries and hybrid capacitors. *Energy Storage Materials* **2020,** *25*, 636-643.

86. Hu, J.; Zhang, C.; Zhang, Y.; Yang, B.; Qi, Q.; Sun, M.; Zi, F.; Leung, M. K. H.; Huang, B., Interface Modulation of MoS2/Metal Oxide Heterostructures for Efficient Hydrogen Evolution Electrocatalysis. *Small* **2020,** *16* (28), 2002212.

87. Wang, X. H.; Zheng, C. C.; Ning, J. Q., Influence of curvature strain and Van der Waals force on the inter-layer vibration mode of WS2 nanotubes: A confocal micro-Raman spectroscopic study. *Scientific Reports* **2016,** *6* (1), 33091.

88. Li, M.; Cai, B.; Tian, R.; Yu, X.; Breese, M. B.; Chu, X.; Han, Z.; Li, S.; Joshi, R.; Vinu, A., Vanadium doped 1T MoS2 nanosheets for highly efficient electrocatalytic hydrogen evolution in both acidic and alkaline solutions. *Chemical Engineering Journal* **2021,** *409*, 128158.

89. Choudhary, N.; Li, C.; Chung, H.-S.; Moore, J.; Thomas, J.; Jung, Y., High-Performance One-Body Core/Shell Nanowire Supercapacitor Enabled by Conformal Growth of Capacitive 2D WS2 Layers. *ACS Nano* **2016,** *10* (12), 10726-10735.

90. Li, L.; Gao, J.; Cecen, V.; Fan, J.; Shi, P.; Xu, Q.; Min, Y., Hierarchical WS2@NiCo2O4 Core–shell Heterostructure Arrays Supported on Carbon Cloth as High-Performance Electrodes for Symmetric Flexible Supercapacitors. *ACS Omega* **2020,** *5* (9), 4657-4667.

91. Mugheri, A. Q.; Otho, A. A.; Mugheri, A. A., Meritorious spatially on hierarchically Co3O4/MoS2 phase nanocomposite synergistically a high-efficient electrocatalyst for hydrogen evolution reaction performance: Recent advances & future perspectives. *International Journal of Hydrogen Energy* **2021,** *46* (44), 22707-22718.

92. Ariga, K. Nanoarchitectonics: Method for everything in material science. *Bulletin of the Chemical Society of Japan*, in press. DOI: 10.1093/bulcsj/uoad001.

ToC Graphic

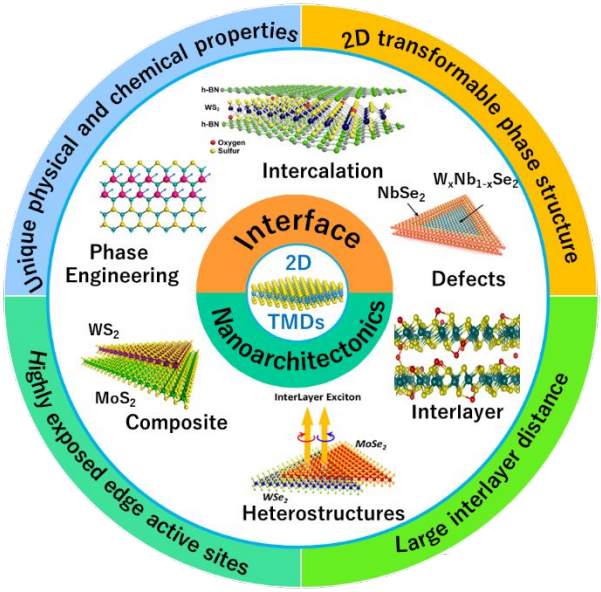
Unique physical and chemical properties
2D transformable phase structure
Large interlayer distance
Highly exposed edge active sites
Interface
2D
TMDs
Nanoarchitectonics
Intercalation
Phase Engineering
Defects
NbSe2
WxNb1-xSe2
WS2
MoS2
Composite
Interlayer
InterLayer Exciton
MoSe2
WSe2
Heterostructures